

# Evidence for Harmonic Relationships in the High Frequency QPOs of XTE J1550–564 and GRO J1655–40

Ronald A. Remillard and Michael P. Muno  
Center for Space Research, MIT, Cambridge, MA 02139  
rr@space.mit.edu; muno@space.mit.edu

and

Jeffrey E. McClintock  
Harvard-Smithsonian Center for Astrophysics, 60 Garden St. MS-3,  
Cambridge, MA 02138; jem@cfa.harvard.edu

and

Jerome A. Orosz  
Astronomical Institute, Utrecht University, Postbus 80000, 3508 TA Utrecht,  
The Netherlands; J.A.Orosz@astro.uu.nl

## ABSTRACT

We continue to investigate the X-ray timing and spectral properties of the black hole binary XTE J1550–564 during its 1998–1999 outburst. By grouping observations according to the type of low-frequency quasiperiodic oscillation (LFQPO) identified in a previous paper, we show evidence that two high-frequency QPOs (HFQPOs) occur simultaneously near 184 and 276 Hz. In each case, we can model the QPO profiles while assuming that the central frequencies are related by a 3:2 ratio. In one group, there is also evidence of a broad feature at the fundamental frequency of 92 Hz. We also investigate the April 2000 outburst of the source and confirm the suggestion of Miller et al. that a 270 Hz QPO is accompanied by a second feature near 180 Hz. We conclude that the majority of the 28 individual HFQPO detections in XTE J1550–564 are best interpreted as harmonics of a fundamental oscillation near 92 Hz. The most significant exceptions to this pattern are the 143 Hz QPO detected on 1998 October 15 and the 65 Hz QPO reported by Kalemci et al. for 2000 May 20. We next investigate all of the X-ray energy spectra and QPO results for individual observations of XTE J1550–564, and we find a systematic increase in the strength of the power-law component as the stronger of the two HFQPOs shifts from 276 to 184 Hz. A strikingly similar result is

seen in the spectra of GRO J1655–40 when the stronger HFQPO shifts from 450 to 300 Hz. The fundamental HFQPO frequencies for the two X-ray sources scale as  $M^{-1}$ , which is consistent with the hypotheses that these HFQPOs represent some kind of oscillation rooted in general relativity (GR) and that the two black holes have similar values of the dimensionless spin parameter. We discuss physical mechanisms that may explain these HFQPOs. A resonance between orbital and radial coordinate frequencies is one possibility suggested by Abramowicz & Kluzniak. For XTE J1550-564, this would imply moderate values for the dimensionless spin parameter ( $0.1 < a_* < 0.6$ ), with similar results for GRO J1655-40. However, there remain large uncertainties as to whether this model can produce the HFQPOs and their variations in frequency. We also discuss models for “diskoseismic” oscillations. In this case, the concept that the inner disk behaves as a resonance cavity in GR has certain attractions for explaining HFQPOs, but integral harmonics are not predicted for the three types of diskoseismic modes.

*Subject headings:* black hole physics — stars: individual (XTE J1550–564) — stars: individual (GRO J1655–40) —stars: oscillations — X-rays: stars

## 1. Introduction

XTE J1550–564 is a recurrent X-ray nova and a microquasar that has been extensively studied at X-ray and optical frequencies. A major outburst during 1998-1999 revealed complex evolution in both its spectral properties and variability characteristics (Sobczak et al. 2000b; Homan et al. 2001; Remillard et al. 2002). It is one of five black hole candidates that exhibit transient high-frequency QPOs (HFQPOs), while its stronger and more common low-frequency QPOs (LFQPOs) are seen to vary in frequency in response to changes in the spectrum of the accretion disk. Additional X-ray outbursts with weaker maxima and shorter duration were observed in 2000 April to June (Tomsick et al. 2001b; Miller et al. 2001), in 2001 February - March (Tomsick et al. 2001a), and again in 2002 January (Swank, Smith, & Markwardt 2002). The accumulated investment of almost 400 RXTE pointed observations (2-200 keV) provides a unique archive of high-quality monitoring data that span 4 decades in X-ray luminosity, with several excursions through each of the canonical emission states of black hole binaries. These resources motivate continuing efforts to understand the structure of the accretion flow at various levels of X-ray luminosity and to search for effects of general relativity (GR) in the innermost regions of the accretion disk.

Optical photometry of XTE J1550–564 during outbursts revealed the binary period of 1.54 days and the perplexing weakness of an optical response to X-ray flares (Jain et al. 2001). Optical spectroscopy and photometry during accretion quiescence has recently established that the system is a dynamical black hole binary, with a black hole mass of  $10.0 \pm 1.5 M_{\odot}$  (Orosz et al. 2002). The companion star is a late type subgiant (G8IV to K4III), and the binary inclination angle is constrained to the range  $72^{\circ} \pm 5^{\circ}$  (Orosz et al. 2002).

Radio observations revealed a relativistic jet associated with the large X-ray flare of 1998 September 19 (Hannikainen et al. 2001). The radio source then decayed away while the X-ray source remained in the “very high” state. During the X-ray “low-hard” state seen in the outburst of 2000, weaker radio flux was detected with an inverted spectrum, suggesting the presence of a steady jet (Corbel et al. 2001).

In a previous paper (Remillard et al. 2002; hereafter RSMM02), we used 209 RXTE observations of XTE J1550–564 during its 1998–1999 outburst to investigate the relationships between HFQPOs, LFQPOs and the spectral characteristics reported by Sobczak et al. (2000b). It was found that complex LFQPOs are better organized in their correlations with both HFQPOs and the accretion disk flux and temperature when we distinguished three types (“A”, “B”, and “C”) on the basis of phase lags and coherence values measured at the central QPO frequency. The LFQPO types (but not their frequencies) are correlated with the frequencies of HFQPOs that were detected on 20 occasions. Type A LFQPOs (5–10 Hz, broad profiles, lag in soft X-rays) are associated with narrow HFQPOs near 276 Hz. Type B LFQPOs (5–7 Hz, narrow profiles, lag in hard X-rays) correspond to broader HFQPOs near 184 Hz. The common type “C” LFQPOs (variable frequencies, narrow profiles, strong amplitude and harmonics, and small phase lags) coincide on rare occasions with HFQPOs at lower frequencies (100–169 Hz).

There are now five black hole candidates that exhibit transient HFQPOs, and for three of them there is evidence that two HFQPOs can occur simultaneously. HFQPO pairs have been seen in GRO J1655–40 (300, 450 Hz; Strohmayer 2001a; Remillard et al. 1999b), GRS 1915+105 (40, 67 Hz; Strohmayer 2001b), and also probably during the 2000 outburst of XTE J1550–564 (Miller et al. 2001). In the first two cases, Strohmayer (2001a; b) investigated combinations of the azimuthal and radial coordinate frequencies in GR to explain the pair of HFQPOs, noting that other explanations are possible. For the case of GRO J1655–40, it was further claimed (Strohmayer 2001a) that the 450 Hz QPO suggests that the black hole must have substantial spin (i.e. dimensionless spin parameter,  $a_* > 0.15$ ). This conclusion uses the optically determined mass of the black hole (Shahbaz et al. 1999; Greene, Bailyn, & Orosz 2001), along with the assumption that the orbital rotation

frequency (in GR) at the innermost stable circular orbit around the black hole (Shapiro & Teukolsky 1983) is the highest frequency that can be seen in the X-rays emission.

An alternative interpretation for pairs of HFQPOs utilizes “diskoseismology”, which considers adiabatic perturbations in a relativistic accretion disk (Wagoner 1999; Kato 2001). If the HFQPOs in GRO J1655–40 and GRS 1915+105 represent fundamental  $g$ –mode and  $c$ –mode diskoseismic oscillations, then substantially higher values of the spin parameter are derived ( $a_* \sim 0.9$  and  $\sim 0.7$ , respectively; Wagoner, Silbergleit, & Ortega-Rodriguez 2001). For the case of GRO J1655–40, yet another interpretation was offered by Abramowicz & Kluzniak (2001), who hypothesize that there is enhanced X-ray emission at the radius in the accretion disk where there is a resonance between the Keplerian and radial coordinate frequencies. This idea is motivated by the 3:2 integral ratio seen in the frequencies of HFQPOs from that source. When considering all of the HFQPO observations, it is possible that the results may require more than one physical model.

As a followup to RSMM02, we address four questions related to QPO behavior in XTE J1550–564. (1) If we average the power density spectra (PDS) during the 1998-1999 outburst for groups defined by the LFQPO type, is there any evidence for a pair of HFQPOs? (2) Can we confirm the suggestion of Miller et al. (2001) that HFQPOs near 180 Hz and 270 Hz occur simultaneously during the outburst of 2000? (3) Are the pairs of HFQPOs in XTE J1550–564 and GRO J1655–40 related precisely by a 3:2 ratio? (4) Are there X-ray spectral properties that distinguish the observations when the upper or lower HFQPO is stronger in each of these two sources?

## 2. Observations and Data Analysis

We continue the analysis of XTE J1550–564 using RXTE observations reported in previous publications. For the 209 observations of the 1998-1999 outburst, spectral parameters were tabulated by Sobczak et al. (2000b). QPO properties are given in RSMM02. Timing results for 19 observations (XTE program P50134) during the outburst of 2000 April-May are reported by Miller et al. (2001). We supplement these with analyses of contemporaneous exposures under RXTE programs P50135 (37 observations) and P50137 (11 observations), which are now publicly available.

We elaborate on our methods for conducting error analysis for features in the PDS, since the significance of QPOs is an important topic in §3. As noted in RSMM02, the PDS ( $P_\nu$  vs.  $\nu$ ) are computed for 256 s data segments and then averaged for each observation. We first compute the PDS using the normalization of Leahy et al. (1983). For each

frequency bin in the discrete Fourier transform ( $\Delta\nu = 2^{-8}$  Hz), we compute the uncertainty as the larger of either the statistical error ( $2/N^{0.5}$ ) or the observed standard deviation of the mean power, where there are  $N$  data segments within the observation. We then subtract the Poisson-corrected dead time, as described in Morgan, Remillard, & Greiner (1997), using the average count rates (per PCU) for good events and for very large events (which have a longer dead time) during a given observation. The PDS are then renormalized by the mean source count rate (i.e. above the non-source background), so that the final PDS has units of (rms deviation / mean)<sup>2</sup> Hz<sup>-1</sup>. We logarithmically rebin the frequencies using intervals that are successively larger by a factor of 1.04, propagating the uncertainty within each frequency interval. When we average the PDS for groups of observations, we compute the weighted mean (using  $\sigma^{-2}$ ) and its uncertainty for each frequency interval.

The PDS are searched for LFQPOs (0.5 to 30 Hz) and HFQPOs (30 to 1000 Hz) separately, using a sliding frequency window that typically spans 0.2 to 5.0  $\nu$ . Within the window, the power continuum ( $P_{cont}$ ) is modeled with a second order polynomial in  $\log \nu$ , since the local power continuum usually resembles a power-law function with a slight amount of broad curvature. The QPO profiles are presumed to be Lorentzian functions, and they are generally distinguished from broad peaks in the power continuum by a coherence parameter,  $Q = \nu/FWHM \gtrsim 2$ . We use  $\chi^2$  minimization to obtain the best fit for the QPO profile and the local power continuum. The uncertainty in the power continuum is estimated via  $\chi^2$  analysis near the best-fit value, and a similar treatment is used to estimate the uncertainties in the QPO central frequency ( $\nu_0$ ) and the  $FWHM$ .

If the inclusion of a QPO feature is statistically warranted, and if the best-fit value of  $\chi^2_\nu$  is acceptable, then we evaluate the significance of the feature with a conservative and empirical approach, as follows. Within the central frequency range of the QPO,  $\nu_0 \pm FWHM$ , we integrate  $P_\nu - P_{cont}$  and then divide the result ( $S$ ) by its statistical uncertainty ( $\sigma_S$ ), where the calculation of  $\sigma_S$  considers, in quadrature, the uncertainties in the power density measurements as well as the continuum fit. Usually,  $\sigma_S$  is dominated by the measurement uncertainty in the power density bins, since there are many bins that constrain the continuum fit. However, QPO searches may be susceptible to systematic errors in the power continuum model (especially for broad QPOs), which are difficult to ascertain. For this reason, and given our practical experience searching for QPOs in many black hole candidates, we judge the threshold for a high level of confidence to be near a significance  $S/\sigma_S \gtrsim 4$  for QPO searches using this method.

When QPO detections are significant, we use the best-fit values for the Lorentzian peak and  $FWHM$  to compute the total integrated power ( $P$ ) in the PDS feature, and the rms amplitude of the QPO is then  $a = P^{0.5}$ . We can then use the QPO significance

as a measure of the uncertainty in  $P$ , leading to an estimate of the amplitude uncertainty,  $\sigma_a/a = 0.5\sigma_S/S$ . We note that the factor of 0.5 was inadvertently neglected in reporting  $\sigma_a$  values (overly large) in Table 1 of Remillard et al. (1999a).

We note that global PDS modeling has been performed successfully for sources in hard X-ray states using multiple Lorentzians (Nowak 2000; Pottschmidt et al. 2002). The results yield broad profiles ( $Q < 0.5$ ), which distinguish these features as broad power peaks rather than QPOs. We note, however, that the multiple-Lorentzian model generally does not work well for PDS associated with the “high” or “very high” states where the power continuum roughly resembles a power-law function over several decades in frequency. This is the case for most of the observations of XTE J1550–564 that exhibit HFQPOs, and therefore a more localized fit for the power continuum is a practical necessity.

### 3. Results

We show the results for investigations of the four questions raised in the §1. All of the power density spectra are displayed in units of  $\log(\nu \times P_\nu)$  vs.  $\log(\nu)$ , thereby making it easier to see peaks in the power density and to evaluate the relative strengths of features at widely different frequencies (Psaltis, Belloni, & van der Klis 1999; Nowak 2000). We note, however, that all of the QPO fits are computed in the  $(P_\nu, \nu)$ -plane.

#### 3.1. PDS of XTE J1550–564 during 1998-1999, Averaged by LFQPO Type

Using Table 1 of RSMM02, we computed the average power spectra of XTE J1550–564 (6 to 30 keV) for groups of observations that show LFQPO types A (10 cases), B (9 cases), and C (44 of 46 cases that have data in this energy band). Observations classified “A?” were included in the A group, but the five “C’ ” cases that followed the 7.7 Crab flare were not included in the C group. The results are shown in Fig. 1. We have utilized the energy range 6 to 30 keV for this analysis, because this energy range optimizes the detections of the various HFQPOs seen in XTE J1550–564. Analogous investigations at 2 to 30 keV or 13 to 30 keV produce similar conclusions with weaker statistics.

In RSMM02, the the broad type A LFQPOs (5–10 Hz with phase lags in soft X-rays) were associated with a narrow HFQPO near 280 Hz. In Fig. 1 this HFQPO is the strongest feature in the average PDS (top panel), while there is also evidence of a weak feature near 185 Hz which is not detected during any individual observation. The narrow type B LFQPOs (5–7 Hz, strong harmonics, hard lags) are associated with a broader HFQPO near

185 Hz. In Fig. 1, the average B-type PDS clearly shows the LFQPO, its harmonics at  $0.5\nu_0$  and  $2\nu_0$ , and the strong peak at 185 Hz. There is also complex structure and possibly additional HFQPOs on both sides of the 185 Hz feature. Type C LFQPOs ( $\nu_0$  varying from 0.08 to 7 Hz, weak phase lags) are smeared out in the average C-type PDS, which is dominated by a continuum that may be deconvolved into three or more broad power peaks. For the C-type PDS, the integrated rms fractional variability (0.1 to 1000 Hz) is 0.21 at 6-30 keV, while the total power for types A and B is only 0.04 to 0.08 at 6-30 keV. Finally, the 4th panel of Fig. 1 shows the PDS for 1998 September 19, when XTE J1550–564 was in the midst of a flare to a peak intensity of 7 Crab (see e.g. Sobczak et al. 2000b). Significant QPOs are seen at 4.9, 13.2, and 183 Hz on that occasion.

To quantify the significance of the weaker high-frequency features in the type A and B average PDS, we modeled the data in the range 40-1200 Hz according to the procedures described in §2. In each of these fits, the central frequencies are forced to have ratios of 2:3 or 1:2:3, and their positions are adjusted with one free parameter. The results are shown in Fig. 2. The top two panels show QPO fits for the type A and B groups; the PDS data are the same as those plotted in Fig. 1. The best fit models for the QPO profiles are shown with dark lines, the power continuum is shown with a dashed line, and the central QPO frequencies in the model are shown with vertical ticks above the data. We note that our dead time correction model chronically leaves residual power at the level of  $P_\nu \sim 10^{-6} \text{ Hz}^{-1}$  (see Revnivtsev, Gilfanov, & Churazov 2000 for further discussions of this effect). Thus, with the PDS displayed in  $\log(\nu \times P_\nu)$  units, the power continuum (dashed line) shows some upward curvature while smoothly connecting the source power at 50 Hz to the residual dead time effects at 1 kHz.

All of the QPO parameters derived from these profile models are given in Table 1. The significance of the 187 Hz QPO in the average type A PDS is near  $4 \sigma$ , as is the shallow QPO found at 92 Hz in the type B PDS. We note that these are near the level deemed to be reliable for general QPO searches. We conclude that there is sound evidence for harmonic relationships in the HFQPOs in XTE J1550–564, but we also acknowledge the need for confirmation of these results for this source and for other black hole binaries as well. The type B PDS seems to exhibit the highest harmonic content. We note the hints of weak features seen at the 4th and 5th harmonics ( $2.4 \sigma$  and  $2.0 \sigma$ , respectively) as shown with arrows in Fig. 2.

### 3.2. HFQPOs in XTE J1550–564 during the Outburst of 2000

We also examine data from the second outburst of XTE J1550–564 that began around 2000 April 4. Miller et al. (2001) reported six detections of a QPO near 270 Hz out of a total of 12 RXTE observations that were made between 2000 April 30 and May 9. This time interval occurs just after the time of maximum luminosity (April 29), as seen with the RXTE All Sky Monitor. In the average PDS for these 6 observations, QPOs were found at  $268 \pm 3$  Hz ( $7.8 \sigma$ ) and  $188 \pm 3$  Hz ( $3.5 \sigma$ ), suggesting that the features appear simultaneously (Miller et al. 2001).

Here, we add two details to the findings of Miller et al. (2001), who reported strong HFQPO detections by selecting PCA data above 6 keV. First, we find one additional HFQPO detection at  $267 \pm 8$  Hz ( $Q = 4.9$ ) on 2000 May 5. The significance is highest ( $4.5\sigma$ ) for data in the energy range 2 to 30 keV. Second, for the five remaining observations during 2000 April 30 to May 9, we find that their average PDS contains a significant QPO near 270 Hz. We therefore combine all 12 observations (6 to 30 keV) to further test the significance of a second QPO near 180 Hz and to help judge the acceptability of a model with forced harmonic relationships in the central frequencies. The results (Fig. 2 and Table 1) support the conclusion by Miller et al. that the pair of QPOs occur simultaneously, and the significance of the second QPO near 180 Hz is increased to  $5.0 \sigma$  by averaging together all 12 observations.

The central frequencies (independently fit) derived by Miller et al. (2001) deviate from a ratio of 3:2 by  $2.2 \sigma$ . For the 12 observations in the same time interval (bottom panel of Fig. 2), the harmonic fit is acceptable. Comparing the QPO profile model with the data, one can see that the peak at lower frequency might move to slightly higher frequency if it were treated as a free parameter. Since the six QPO detections (Miller et al. 2001) decrease in central frequency with time (276 to 249 Hz), small deviations from a 3:2 frequency ratio could arise from changes in the relative strength of the two features during the sampling interval. We conclude that the QPO properties during the 2000 outburst of XTE J1550–564 are amenable to interpretation via a harmonic relationship, but alternative possibilities cannot be excluded.

### 3.3. Summary of HFQPOs in XTE J1550–564

There are now 28 HFQPO detections reported for individual observations of XTE J1550–564 (Homan et al. 2001; RSMM02; Miller et al. 2001; Kalemci et al. 2001; §3.2). Their central frequencies vary substantially, but the majority tend to cluster near



184 or 276 Hz. This is evident in the histogram of HFQPO frequencies shown in Fig. 3 (top panel). In making the histogram, we varied the binning intervals to maintain a width of  $\pm 5\%$  relative to the central frequency.

None of the individual observations yield detections of a pair of HFQPOs, yet when groups of observations are averaged, either by the LFQPO type (1998-1999) or by time interval (2000), we find three HFQPOs organized as harmonics near 92, 184, and 276 Hz. These results suggest that the HFQPO harmonics appear simultaneously, but that only the dominant feature is detectable in the individual observations.

We next assess the extent to which any individual HFQPO detections occur well outside of this harmonic scheme. In most cases (17 of 28), the allowed range of frequencies ( $\nu \pm 1\sigma$ ) lies within 3% of a harmonic value. At the other extreme, 3 of 28 cases deviate from a harmonic value by an amount greater than 12%. One of these is the 65 Hz QPO reported by Kalemci et al. (2001) for 2000 May 20. The two others were observed on 1998 October 15 (with type C LFQPOs), and their average PDS is shown in Fig. 4. The QPO ( $5.0\sigma$ ) is found at  $143 \pm 8$  Hz, which is closer to the geometric mean of the harmonics than it is to either 92 or 184 Hz. Even though the statistical quality of the data is limited, it is important to note that the harmonic scheme may represent only a subset of the behavior patterns of HFQPOs in XTE J1550–564.

### 3.4. X-ray Spectra and HFQPOs in XTE J1550–564

We now focus attention on the spectral properties that may distinguish which harmonic frequency is present in each observation that exhibits an HFQPO. XTE J1550–564 displays a typical X-ray spectrum for a black hole binary, with a thermal component from the accretion disk and a hard power-law attributed to inverse Compton scattering by electrons of unknown origin. Sobczak et al. (2000b) deconvolved these spectral components and reported parameters for the 209 RXTE observations obtained during the 1998-1999 outburst. We performed the same analysis for the 43 RXTE observations obtained during 2000 in order to compare the behavior of the source during the two outbursts.

It has been shown that the exercise of plotting the integrated disk flux versus power-law flux in black hole binaries is very useful in tracking the flow of energy between the two components through different X-ray states, and also in relating QPO parameters to spectral parameters (Muno, Morgan, & Remillard 1999; Sobczak et al. 2000a). Using the spectral parameters of Sobczak et al. (2000b), we show the flux measures in the two spectral components during the 1998-1999 outburst in Fig. 5. As discussed in RSMM02, one

can integrate the spectral components either over the PCA energy range with highest sensitivity (2-25 keV) or over bolometric limits, in which case the majority of the disk flux is extrapolated below 2 keV. Both options are displayed in Fig. 5. For the bolometric estimates, the lower limit on the integration of the power-law component is reduced to 1 keV, which affects the results significantly when the power law spectrum is steep.

We note that the bolometric disk flux is  $2.16 \times 10^{-11} N_{dbb} T^4 \text{ erg cm}^{-2} \text{ s}^{-1}$ , where  $N_{dbb}$  is the multi-temperature disk normalization:  $N_{dbb} = R_{in} \cos\theta / d^2$ , with the inner disk radius,  $R_{in}$ , expressed in km and the distance,  $d$ , in units of 10 kpc. Assuming a disk inclination  $\theta = 72^\circ$  and  $d = 6 \text{ kpc}$  (Orosz et al. 2002), then the bolometric disk luminosity would be  $1.3 \times 10^{39} \text{ erg s}^{-1}$  (or  $1.0 L_{Edd}$  for a  $10 M_\odot$  black hole) for a value of  $17.9 \times 10^{-8} \text{ erg cm}^{-2} \text{ s}^{-1}$  in the left panel (horizontal axis) in Fig. 5. For the power-law component, the luminosity depends only on  $d$ , and the corresponding value (vertical axis) is  $29.2 \times 10^{-8} \text{ erg cm}^{-2} \text{ s}^{-1}$ .

In Fig. 5, we use the symbol color to denote the following QPO conditions: HFQPO detections (blue), LFQPOs only (green “x”), and no QPOs (red “x”). In addition, the shape of the blue symbols distinguishes the HFQPOs near 92 Hz (triangle), 184 Hz (filled square), and 276 Hz (star). The results for the pair of observations on 1998 October 15 are displayed with blue circles. There are clear patterns in these results, and the conclusions do not depend on the integration limits used to calculate the flux (compare left and right panels). There is a fairly well defined horizontal branch (red “x”s) in which the disk dominates the spectrum and no QPOs are seen, just as in the case of GRS 1915+105 (Muno, Morgan, & Remillard 1999). The large majority of vertical excursions from this branch display some kind of QPO activity. These spectra with enhanced power-law flux occur over a wide range of disk flux, in contrast with the vertical branch at very low disk flux in the case of GRS 1915+105 (Muno, Morgan, & Remillard 1999).

The spectral diagrams in Fig. 5 also distinguish the HFQPOs and the selection of different harmonic frequencies at different times. There is a systematic difference in magnitude of the power-law flux between the points associated with the 276 Hz QPO (stars) versus the 184 Hz QPO (solid squares). The X-ray spectra associated with the 276 Hz QPO lie systematically closer to the horizontal branch in which the spectrum is dominated by the accretion disk.

We present the same diagrams for the much weaker outburst of 2000 in Fig. 6. This outburst samples different X-ray states and reaches a maximum luminosity that is a factor of 10 below the levels seen during 1998-1999. Here, all of the HFQPO detections associated with the 276 Hz feature (blue stars) occur at approximately the same disk and power-law fluxes as their counterparts in Fig. 5, and they again lie close to the disk-dominant branch (red x’s) plotted in Fig. 4. The observations during the time interval of 2000 April 30 - May

9 correspond to the 12 red and blue points in the lower-right quadrant of the right panel in Fig. 6. We have shown that the average PDS for these observations exhibits a strong QPO at 270 Hz accompanied by a  $5\sigma$  detection at 180 Hz (Fig. 2 and Table 1). We conclude that these spectral and temporal results for the 2000 outburst support the idea that HFQPOs near 184 Hz and 276 Hz represent a temporal signature of accretion that is inherent to this black hole binary system.

Finally, we note that XTE J1550-564 additionally displays a vertical branch (green x's) during the 2000 outburst (Fig. 6) in which the power law component varies while there is little contribution from the disk. At these times the PDS show only LFQPOs and strong continuum power. These observations are further associated with a steady jet seen in the radio band (Corbel et al. 2001). A similar X-ray track associated with a flat radio spectrum has been seen in GRS 1915+105 (Muno, Morgan, & Remillard 1999).

### 3.5. Summary of HFQPOs in GRO J1655–40

HFQPOs near 300 Hz at photon energies of 2 to 30 keV were reported for 6 observations of GRO J1655–40 by Remillard et al. (1999b), (significance  $\gtrsim 3\sigma$ ). The examination of RXTE pointings under programs 10261 and 20187 (which were not available for that paper) yield an additional strong detection ( $6.0\sigma$ ) at  $320 \pm 11$  Hz (with  $Q = 4.6$ ) for the observation on 1996 November 7. There is no detection of a QPO near 450 Hz in this observation.

Strohmayer (2001) reported detections of 5 HFQPOs near 450 Hz for PDS computed using data from photon energies in the range 13 to 27 keV. Again, the analysis of the data from these other programs yields an additional, weak detection ( $3.4\sigma$  at 13 to 27 keV) at  $447 \pm 5$  Hz (with  $Q = 8.9$ ) for the observation on 1996 June 20. There is no 300 Hz QPO detection during that observation.

These results raise the total to 10 observations in which one or more HFQPOs are detected in GRO J1655–40: 4 show only the 300 Hz QPO, 3 show only the 450 Hz QPO, and 3 show both. For the three observations that exhibit both HFQPOs (Strohmayer 2001a), the independent profile fits (using different energy bands) yield central frequencies of  $295 \pm 4$  Hz (2-30 keV) and  $440 \pm 5$  Hz (13-30 keV), respectively. These results are consistent with a 3:2 ratio, as noted in §1, while one feature is usually much stronger than the other, as seen in the behavior of XTE J1550–564. In the next section, we examine whether the X-ray spectra evolve in parallel with the relative strength of the HFQPO features in the case of GRO J1655–40.

### 3.6. X-ray Spectra and HFQPOs in GRO J1655–40

We use the 52 spectral observations reported by Sobczak et al. (1999), supplemented by similar analyses for RXTE programs 10261 (six spectra binned in 1-day intervals), 20187 (1996 November 7), and 20402 (the final three observations, not reported previously). In addition, since there is so much exposure time during 1996 May 9–11, we choose to sample the data in 7 time intervals, rather than in 3 daily bins. This yields a net of 66 spectral observations of GRO J1655–40. We display the results of the spectral decomposition in Fig. 7. The procedures are the same as those conducted for XTE J1550–564, except that we use an inclination angle of  $70^\circ$  and a distance of 3.2 kpc for GRO J1655–40 (Greene, Bailyn, & Orosz 2001 and references therein). In this case, the disk luminosity would be  $7.9 \times 10^{38}$  erg s $^{-1}$  (or  $1.0 L_{Edd}$  for a  $6.3 M_\odot$  black hole) for a bolometric disk flux of  $45 \times 10^{-8}$  erg cm $^{-2}$  s $^{-1}$  in the left panel (horizontal axis) of Fig. 7. For the power-law component, the same luminosity corresponds to  $65 \times 10^{-8}$  erg cm $^{-2}$  s $^{-1}$  in the same Figure panel (vertical axis).

For GRO J1655–40, the relationship between HFQPO properties and the energy division between the spectral components resembles the results for XTE J1550–564 in several important ways. The observations with HFQPOs (blue symbols) lie above the horizontal branch (red “x”s) where the disk dominates the spectrum and no QPOs are seen. Moreover, with increasing power-law luminosity we see the following progression: first are the observations where we detect only the 450 Hz QPO (open stars), next are cases in which both HFQPOs are detected simultaneously (filled stars), finally there are those in which only the 300 Hz QPO is seen (solid squares). This is the same pattern seen for XTE J1550–564, where the strongest modulation shifts from 276 to 184 Hz as the power-law flux increases (cf. Fig. 5). This similarity suggests that the physical process that produces HFQPOs in these two sources is identical.

## 4. Discussion

The 3:2:1 frequency ratio with a fundamental frequency near 92 Hz seems to account for most of the X-ray HFQPOs detected in 28 individual observations of XTE J1550–564. The features seen in the average PDS for three well-defined groups of observations support this scheme and further suggest that the HFQPO harmonics may coexist. Moreover, all of the 13 HFQPO detections (in 10 observations) in GRO J1655–40 conform to a 3:2 frequency ratio with an implied fundamental at 150 Hz, including the three occasions in which both the 300 Hz and 450 Hz QPOs were detected (Strohmayer 2001a). These results provide solid evidence for harmonic relationships between the HFQPOs in black hole binaries; nevertheless we acknowledge the need to confirm this conclusion in these and other X-ray

sources, since many of the detections are near or below the statistical threshold for high levels of confidence.

We have found that the concurrent evolution of the HFQPOs and the X-ray spectra is very similar for the black hole binaries XTE J1550–564 and GRO J1655–40. The primary result is an increase in the luminosity of the X-ray power-law component as the HFQPOs exhibit a shift from the 3rd harmonic to the 2nd harmonic. We also note that HFQPOs are generally not detected along the spectral tracks in which either the accretion disk or the power-law component strongly dominates the spectrum (i.e. the horizontal, red tracks in Figs. 5 and 7 and the vertical, green track in Fig. 6). The energy decomposition diagrams do not show perfect segregation of points relative to the HFQPO properties. However, we cannot expect perfect organization, given the variations in statistical sensitivity and the faintness of the HFQPOs (rms amplitudes of 0.5% to 5% of the mean count rate in the selected energy band).

The deduced fundamental frequencies for the HFQPOs in XTE J1550–564 (92 Hz) and GRO J1655–40 (150 Hz) differ by a factor of  $1.63 \pm 0.06$ . On the other hand, the inverse ratio of black hole masses is  $1.59 \pm 0.27$  (Orosz et al. 2002 ; Greene, Bailyn, & Orosz 2001), which suggests that the fundamental frequencies scale as  $M^{-1}$ . This result is generally consistent with the known mechanisms related to disk oscillations in the strong-field regime of general relativity, as long as the values of the spin parameter ( $a_*$ ) are similar for these two black holes. These results illustrate both the quantitative value of HFQPO detections as a means of probing the physical properties of black holes, and also the need to continue efforts to independently measure black hole masses via dynamical optical studies.

If these HFQPOs are indeed harmonically related, then we must attempt to specify a physical model that can account for the value of the fundamental frequency, an emission mechanism that produces HFQPOs especially at the 2nd and 3rd harmonics, and an explanation for the spectral evolution associated with the harmonic order. The results for XTE J1550–564 further suggest the need to accommodate occasional shifts in the frequency system (e.g.  $\sim 10\%$  shifts occur  $\sim 15\%$  of the time and perhaps  $\sim 30\%$  shifts occur on rare occasions). With regard to the largest shifts, it is also possible that some HFQPOs involve a different physical mechanism, as suggested for the HFQPO pair at 40 and 67 Hz (i.e., not harmonically related) in GRS 1915+105 (Strohmayer 2001b). Finally, if the oscillations originate in the inner accretion disk, there is a need to understand why there are no HFQPOs seen when the accretion disk dominates the spectrum (red x’s in Figs. 5 and 7). Below we discuss two types of inner disk oscillations, while noting that we cannot exclude the possibility that high frequency oscillations are rooted in the physics of the corona that is responsible for the power-law component.

#### 4.1. Resonance in GR Coordinate Frequencies in the Inner Disk

At the radii in the accretion disk where most of the X-rays originate, the coordinate frequencies in GR are predicted to have non-integral ratios. The 3:2 frequency ratio in the HFQPOs in GRO J1655–40 was therefore seen by Abramowicz & Kluzniak (2001) as remarkable support for their idea that QPOs may result from a resonance between the orbital (i.e., azimuthal) and radial coordinate frequencies in the inner disk. Unlike the orbital and polar frequencies, the radial coordinate frequency reaches a maximum value at a radius larger than the innermost stable orbit, regardless of the values of black hole mass and spin (see Kato 2001; Merloni et al. 2001; and references therein). For a wide range in the spin parameter,  $a_*$ , one can find a particular radius that corresponds to a 1:2 or 1:3 ratio in the radial and orbital coordinate frequencies. In the resonance model, nonlinear perturbations may grow at these radii, ultimately producing X-ray oscillations that represent some combination of the individual resonance frequencies, their sum, or their difference. The proper interpretation of observed HFQPO frequencies may then constrain the black hole spin parameter, if the mass is known via dynamical studies of the binary companion. For GRO J1655–40, Abramowicz & Kluzniak (2001) constrain the spin parameter to the range  $0.2 < a_* < 0.67$  for a black hole mass in the range 5.5 to 7.9  $M_\odot$ . For the same limits in black hole mass and spin, the resonance radius occurs in the range 4.1-7.2  $R_g$ , where  $R_g = GM/c^2$ . We calculate that the resonance radius in these cases lies in-between the innermost stable orbit (3.5-5.3,  $R_g$ ) and the radius of maximum surface emissivity (5.4-8.4  $R_g$ ; Merloni et al. 2001; Zhang, Cui, & Chen 1997). Resonance may therefore occur near radii already expected to yield X-ray emission.

For the case of XTE J1550-564, a black hole mass of 8.5 to 11.5  $M_\odot$  (Orosz et al. 2002) can be combined with the HFQPO oscillations to constrain the value of  $a_*$  using the resonance model, as shown in the top panel of Fig. 8. The blue tracks show values of black hole mass and spin that produce orbital and radial coordinate frequencies that are within 2% of 184 and 92 Hz (left track), respectively, or 276 and 92 Hz (right track), respectively. This model yields limits on the black hole spin:  $0.1 < a_* < 0.6$ . At the lower spin limit (8.5  $M_\odot$  and the 2:1 resonance), the resonance radius is 7.5  $R_g$ , while the innermost stable orbit is 5.6  $R_g$  and a maximum surface emissivity (with no resonance) would occur at 8.8  $R_g$ . At the spin upper limit (11.5  $M_\odot$  and a 3:1 resonance) the resonance occurs at 4.5  $R_g$ , with a last stable orbit of 3.9  $R_g$  and maximum surface emissivity at 6.0  $R_g$ .

In the lower panel of Fig. 8, we illustrate the resonance tracks for GRO J1655–40 for the range 5.8-6.8  $M_\odot$  (Greene, Bailyn, & Orosz 2001) that correspond to orbital and radial coordinate frequencies within 2% of 300 and 150 Hz (left track), respectively, and 450 and 150 Hz (right track), respectively. The resonance model yields  $0.24 < a_* < 0.58$  for

GRO J1655–40. The results of Abramowicz & Kluzniak (2001) differ slightly because they used broader mass constraints ( $5.5\text{-}7.9 M_{\odot}$ ; Shahbaz et al. 1999).

In both X-ray sources the HFQPO detections occur with simultaneous LFQPO detections, such as the 5.8 Hz QPO for the type A PDS and the 6.4 Hz QPO for type B PDS in XTE J1550–564 shown in Fig. 1. In the case of GRO J1655–40, there is more than one LFQPO present in some observations (Remillard et al. 1999b), and we select the QPO at 12.2–17.5 Hz that is very strong in the highest energy band, since it is present in all of the observations that exhibit the HFQPO at either 300 or 450 Hz. We have examined all of the coordinate frequencies and their beat frequencies at the resonance radii consistent with the HFQPOs in each of the two sources. We conclude that the 2:1 resonances, but not the 3:1 resonance, can possibly account for the observed LFQPO frequencies as a beat between the orbital and polar coordinate frequencies. This beat frequency is a precession known as “frame-dragging” (e.g. Merloni et al. 2001). In the top panel of Fig. 8, the regions shaded with darker blue show the subset of resonance parameters for XTE J1550–564 in which the frame-dragging frequency lies in the range 5.8–6.4 Hz. Similarly for GRO J1655–40, in the bottom panel of Fig. 8, the darker blue region shows black hole parameters for which the frame dragging frequency is in the range 12.2–17.5 Hz. We caution that the identification of particular LFQPO features with relativistic frame dragging is, at this point, highly speculative.

Thus far, there is no detailed description as to how a resonance between the orbital and radial coordinate frequencies in GR would produce the requisite X-ray oscillations and the alternating conditions that cause the 2nd or 3rd harmonic to become the dominant QPO. Perhaps even more challenging is the evidence for frequency jitter in the HFQPOs of XTE J1550–564. Because the radial dependence of the two relevant coordinate frequencies is so different, the resonances must be confined to a narrow range in radius. This is a particular problem for the 3:1 resonance, where the ratio of the orbital to radial coordinate frequencies changes rapidly with radius. We illustrate the diverging coordinate frequencies in Fig. 9. in the case of a  $10 M_{\odot}$  black hole with  $a_* = 0.465$  (top panel), a 276:92 Hz resonance occurs at  $5.03 r_g$ ; these mass and spin values are within the 3:1 resonance (right track) shown in Fig. 8 (top panel). Here, a shift in the orbital frequency by  $\pm 10\%$  implies that the radius must vary between 4.7 and  $5.4 r_g$ , and the ratio of coordinate frequencies would then vary in the range 2.5–4.1. It may then be impossible to shift the radius of the perturbation enough to match the shifted HFQPOs and yet maintain the perturbation (no longer in resonance) throughout an RXTE observation, which is longer than the dynamical time by a factor of  $\sim 10^6$ . The problem is less serious, but nontrivial, for the 2:1 resonance (see Fig. 9): for the same black hole mass and  $a_* = 0.324$  (consistent with a 184:92 Hz resonance at  $6.72 r_g$ ), a 10% frequency shift corresponds to a range of radii of 6.3–7.2  $r_g$ ,

over which the ratio of coordinate frequencies changes by about  $\pm 20\%$ .

Finally, we note that all of the QPO models suffer from the ongoing uncertainty as to the origin and geometry of the X-ray power-law component, widely attributed to inverse Compton scattering of thermal photons. We cannot posit a simple way in which the resonance model can appear to shift harmonics in response to increased Comptonization.

## 4.2. Diskoseismic Oscillation Models

A different model that warrants consideration with respect to harmonic HFQPOs in black hole binaries is the diskoseismic model (Kato & Fukue 1980; Wagoner 1999; Kato 2001; Wagoner, Silbergleit, & Ortega-Rodriguez 2001). Here, GR theory predicts that the inner accretion disk may trap oscillations, which is a consequence related to the turnover in the radial coordinate frequency at small radii, which was noted previously. The concept of a resonance cavity in the inner disk is naturally attractive with respect to our interpretation of harmonically related HFQPOs. The three dimensional character of the model allows for modest shifts in oscillation frequency, e.g. with changes in disk thickness and luminosity (Wagoner 1999). Such changes in disk conditions would, in principle, produce coupled changes in both the X-ray spectrum and the oscillation frequency.

The strongest oscillations are expected to arise from gravity modes (“g-modes”), which were investigated in Kerr geometry by Perez et al. (1997). For adiabatic perturbations, the eigenfunction solution predicts a fundamental radial mode ( $m = 0$ ) that would be in the range  $\sim 70$  to  $110$  Hz for a  $10 M_{\odot}$  black hole with  $0 < a_* < 0.5$ . However, for higher  $m$ -number, the g-mode frequencies do not increase by integral values (Perez et al. 1997), and so the predictions do not match the observed HFQPO frequencies. It was noted that the ratio of the orbital frequency at the inner disk radius to the fundamental g-mode frequency is close to a value of 3.08 for a wide range in  $a_*$  (Wagoner 1999). However, this may suggest a strong feature at  $\nu$  (i.e. the g-mode oscillation) and a weak feature near  $3\nu$ , which does not resemble the observations. Investigations have also been made for diskoseismic p-modes (Ortega-Rodriguez & Wagoner 2000) and c-modes (Silbergleit, Wagoner, & Ortega-Rodriguez 2001), but neither study predicts a system of linear harmonics. Kato (2001) has pointed out that the results of numerical simulations and eigenmode analyses show some differences, and therefore further study is warranted.

Partial support for R.R. and M.M. was provided by the NASA contract to M.I.T. for RXTE instruments. J.M. acknowledges the support of NASA grant NAG5-10813. Radleigh Santos helped to process RXTE data for the 2000 outburst of XTE J1550-564. We thank



Michiel van der Klis and Al Levine for providing helpful comments.

## REFERENCES

- Abramowicz, M. A., & Kluzniak, W., 2001, *A&A*, 374, L19
- Corbel, S. et al. 2001, *ApJ*, 554, 43
- Greene, J., Bailyn, C. D., & Orosz, J. A. 2001, *ApJ*, 554, 1290
- Hannikainen, D., Wu, K., Campbell-Wilson, D., Hunstead, R., McIntyre, V., Lovell, J., Reynolds, J., Tzioumis, T., & Wu, K, 2001, *Ap&SS*, 276, 45
- Homan, J., Wijnands, R., van der Klis, M., Belloni, T., van Paradijs, J., Klein-Wolt, M., Fender, R., & Méndez, M. 2001, *ApJS*, 132, 377
- Jain, R., Bailyn, C. D., Orosz, J. A., McClintock, J. E., Sobczak, G. J., & Remillard, R. A. 2001, *ApJ*, 546, 1086
- Kalemci, E., Tomsick, J. A., Rothschild, R. E., Pottschmidt, K., & Kaaret, P. 2001, *ApJ*, 563, 239
- Kato, S. 2001, *PASJ*, 53, 1
- Kato, S., & Fukue, J. 1980, *PASJ*, 32, 377
- Leahy, D., Darbro, W., Weisskopf, M. C., Kahn, S., Sutherland, P. G., & Grindlay, J. E. 1983, *ApJ*, 266, 160
- Merloni, A., Vietri, M., Stella, L., & bini, D. 2001, *MNRAS*, 304, 155
- Miller, J. M., et al. 2001, *ApJ*, 563, 928
- Morgan, E. H., Remillard, R. A., & Greiner, J. 1997, *ApJ*, 482, 993
- Muno, M. P., Morgan, E. H., & Remillard, R. A. 1999, *ApJ*, 527, 321
- Nowak, M. 2000, *MNRAS*, 318, 361
- Orosz, J. A. et al. 2002; *ApJ*, in press; astro-ph/0112101
- Ortega-Rodriguez, M., & Wagoner, R. V. 2000, *ApJ*, 543, 1060
- Perez, C.A., Silbergleit, A.S., Wagoner, R.V., & Lehr, D.E. 1997, *ApJ*, 476 589

- Pottschmidt, K., et al. 2002, submitted to A&A
- Psaltis, D., Belloni, T., & van der Klis, M. 1999, ApJ, 520, 262
- Remillard, R. A., McClintock, J. E., Sobczak, G. J., Bailyn, C. D., Orosz, J. A., Morgan, E. H., & Levine, A. M. 1999a, ApJ, 517, L127
- Remillard, R. A., Morgan, E. H., McClintock, J. E., Bailyn, C. D., & Orosz, J. A. 1999b, ApJ, 522, 397
- Remillard, R. A., Sobczak, G. J., Munro, M., & McClintock, J. E. 2002, ApJ, 564, 962
- Revnivtsev, M., Gilfanov, M., & Churazov, E. 2000, A&A, 363, 1013
- Shahbaz, T., et al. 1999, MNRAS, 306, 89
- Shapiro, S. L., & Teukolsky, S. A. 1983 *Black Holes, White Dwarfs, and Neutron Stars*, (New York: Wiley)
- Silbergleit, A. S., Wagoner, R. V., & Ortega-Rodriguez, M. 2001, ApJ, 548, 335
- Strohmayer, T. E. 2001, ApJ, 552, L49
- Strohmayer, T. E. 2001, ApJ, 554, L169
- Sobczak, G. J., McClintock, J. E., Remillard, R. A., Bailyn, C. D. & Orosz, J. A. 1999, ApJ, 520, 776
- Sobczak, G. J., McClintock, J. E., Remillard, R. A., Cui, W., Levine, A. M., Morgan, E. H., Orosz, J. A., & Bailyn, C. D. 2000a, ApJ, 531, 537
- Sobczak, G. J., McClintock, J. E., Remillard, R. A., Cui, W., Levine, A. M., Morgan, E. H., Orosz, J. A., & Bailyn, C. D. 2000b, ApJ, 544, 993
- Swank, J., Smith, E., & Markwardt, C. 2002, IAU Circ. 7792
- Tomsick, J. A., Smith, D. A., Swank, J. H., Wijnands, R., & Homan, J. 2001, IAU Circ. 7575
- Tomsick, J. A., Corbel, S., & Kaaret, P. 2001, ApJ, 563, 229
- Wagoner, R. V. 1999, Physics Reports, 311, 259
- Wagoner, R. V., Silbergleit, A. S., & Ortega-Rodriguez, M. 2001, ApJ, 559, L25

Wijnands, R., Homan, J., & van der Klis, M. 1999, *ApJ*, 526, 33

Zhang, S. N., Cui, W., & Chen, W. 1997, *ApJ*, 482, L155

Table 1. QPO Fit Parameters<sup>a</sup>

Parameter	units	1998-99 A	1998-99 B	1998 Sep 19	2000 Apr 30-May 9
No. of Obs.	...	10	9	1	12
Source Intensity	Crab units	0.3–2.0	1.3–1.8	6.5	0.3–1.0
$\chi^2_\nu$	...	0.63	0.72	1.10	0.92
Frequency	Hz	281.7 (1.5)	278.0	...	270.3 (3.0)
Significance	$\sigma$	16.8	4.0	...	15.2
FWHM	Hz	33.6 (2.8)	38.6 (12.0)	...	50.0 (8.0)
Q ( $\nu/FWHM$ )	...	8.4 (0.5)	7.2 (1.3)	...	5.4 (1.0)
Amplitude	rms %	3.12 (0.09)	0.70 (0.09)	...	5.05 (0.17)
Frequency	Hz	187.8	185.3 (3.7)	189.6 (5.1)	180.22
Significance	$\sigma$	3.9	13.7	6.6	5.0
FWHM	Hz	22.0 (6.0)	66.1 (10.3)	49.4 ( 10.4)	32.0 (5.0)
Q ( $\nu/FWHM$ )	...	8.5 (1.6)	2.8 (0.3)	3.8 (0.6)	5.6 (0.8)
Amplitude	rms %	1.19 (0.15)	1.07 (0.08)	1.18 (0.09)	2.27 (0.23)
Frequency	Hz	...	92.7	...	...
Significance	$\sigma$	...	4.1	...	...
FWHM	Hz	...	30.4 (6.0)	...	...
Q ( $\nu/FWHM$ )	...	...	3.0 (0.4)	...	...
Amplitude	rms %	...	0.67 (0.08)	...	...

<sup>a</sup>Uncertainty estimates ( $1 \sigma$  confidence) are given in parentheses. Since the model includes only one free parameter for frequency, the uncertainty in the frequency is listed for the harmonic that dominates the fit. All of the QPO results pertain to the spectral range 6 to 30 keV, while the source intensity is evaluated at 2-10 keV, where  $1 \text{ Crab} = 2.4 \times 10^{-8} \text{ erg cm}^{-2} \text{ s}^{-1}$ .

Fig. 1.— Average power spectra for observations of XTE J1550–564 grouped by the type (A, B, or C) of low-frequency QPOs that were observed during the 1998-1999 outburst. We also show the PDS for the intense 7 Crab flare that was sampled on 1998 September 19.

Fig. 2.— Fits for harmonically related HFQPOs in XTE J1550–564 in power spectra at 6–30 keV. The top two panels show the same data displayed in Fig. 1 (1998-1999 averages for LFQPO types A and B). The bottom panel shows the QPO fit for the average of 12 observations between 2000 April 30 and May 9. In each panel, the tick marks above the data show the central frequencies of significant QPOs. The best fit is shown with a smooth, dark curve, and the power continuum is shown with a dashed line. For the type B group (middle panel), the arrows show the expected locations of the 4th and 5th harmonics.

Fig. 3.— Histogram of HFQPO frequencies for XTE J1550–564 and GRO J1655–40. The binning intervals are varied to maintain a width of  $\pm 5\%$  relative to the central frequency. Each source displays two peaks in the distribution that have a 3:2 ratio in frequency.

Fig. 4.— Average power spectrum for XTE J1550–564 for the two observations made on 1998 October 15. The QPO at  $143 \pm 8$  Hz represents the most significant deviation from the harmonic scheme (92, 184, 276 Hz) that accounts for most of the HFQPO detections in this source.

Fig. 5.— Energy spectrum decomposition for XTE J1550–564 during the 1998-1999 outburst. The flux units are  $10^{-8}$  erg cm $^{-2}$  s $^{-1}$ . The flux from the accretion disk and the X-ray power law are shown in conventions of both bolometric flux (extrapolated; left) and apparent flux (2-25 keV; right). The color of the plotting symbol denotes the QPO conditions: HFQPO detections (blue), only LFQPOs (green “x”), and no QPOs (red “x”). In addition, the shape of the blue symbols distinguishes the HFQPOs near 92 Hz (triangle), 184 Hz (filled square), and 276 Hz (star). The pair of observations on 1998 October 15 are displayed with blue circles. In either flux convention (bolometric or apparent), there is a systematic shift away from disk-dominated track (red x’s) as the detected HFQPO shifts from 276 to 184 Hz.

Fig. 6.— Energy spectrum decomposition for XTE J1550–564 during the outburst of 2000. The flux units are  $10^{-8}$  erg cm $^{-2}$  s $^{-1}$ . The symbols follow the definitions given for Fig. 4. In this outburst there is a track in which the power-law spectrum dominates (green x’s), and the points associated with HFQPOs near 276 Hz (blue stars) are again close to the disk-dominated track shown in Fig. 4.

Fig. 7.— Energy spectrum decomposition for GRO J1655–40 during its outburst of 1996-1997. The flux units are  $10^{-8}$  erg cm $^{-2}$  s $^{-1}$ . The symbols follow the definitions given for Fig. 4, except that the observations that exhibit both HFQPOs (300 and 450 Hz) are shown

with solid stars. The results are very similar to those for XTE J1550–564 (Fig. 4). There is increasing power-law flux as the strongest HFQPO shifts from the 450 Hz feature (open stars) to the 300 Hz feature (solid squares).

Fig. 8.— Application of the coordinate-frequency resonance model to the HFQPOs in XTE J1550–564 (top) and GRO J1655–40 (bottom). At each point in the blue shaded regions, the orbital and radial frequencies are within 2% of the HFQPO harmonic frequencies. In each panel, the left track corresponds with the 2:1 resonance (i.e. 184 : 92 Hz in the top panel and 300 : 150 Hz in the bottom panel), and the right track corresponds with the 3:1 resonance (276 : 92 Hz and 450 : 150 Hz, respectively). The regions shaded with darker blue show the parameters that additionally yield a frame-dragging frequency in the range of 5.8-6.4 Hz (top) and 12.2-17.5 Hz (bottom). We caution that the association of LFQPOs with the frame-dragging frequency is highly speculative.

Fig. 9.— Frequencies predicted by GR as a function of radius, for cases that illustrate a 3:1 resonance (top) and a 2:1 resonance (bottom) between the orbital (solid curve) and radial (dashed curve) coordinate frequencies. In each case the mass is  $10 M_{\odot}$  and the spin parameter has been chosen to match the resonances to the values 276:92 Hz and 184:92 Hz, respectively. In each case, the gradients in the coordinate frequencies have opposite signs, and this creates a narrow region in radius where the frequency ratio is near an integral value. Shifts in the observed frequencies may therefore be very difficult to accommodate in the resonance model, especially for the 3:1 resonance.

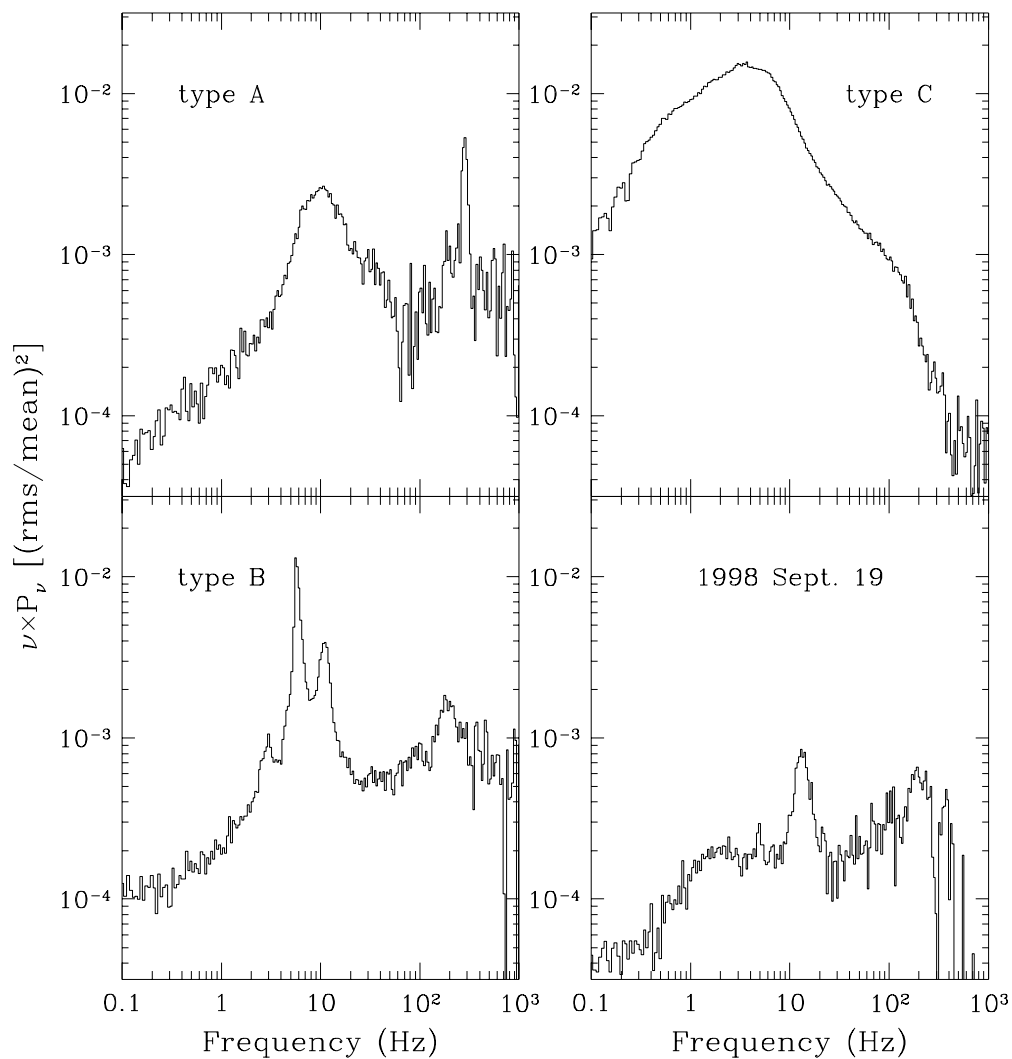


Fig. 1.— Average power spectra for observations of XTE J1550–564 grouped by the type (A, B, or C) of low-frequency QPOs that were observed during the 1998–1999 outburst. We also show the PDS for the intense 7 Crab flare that was sampled on 1998 September 19.

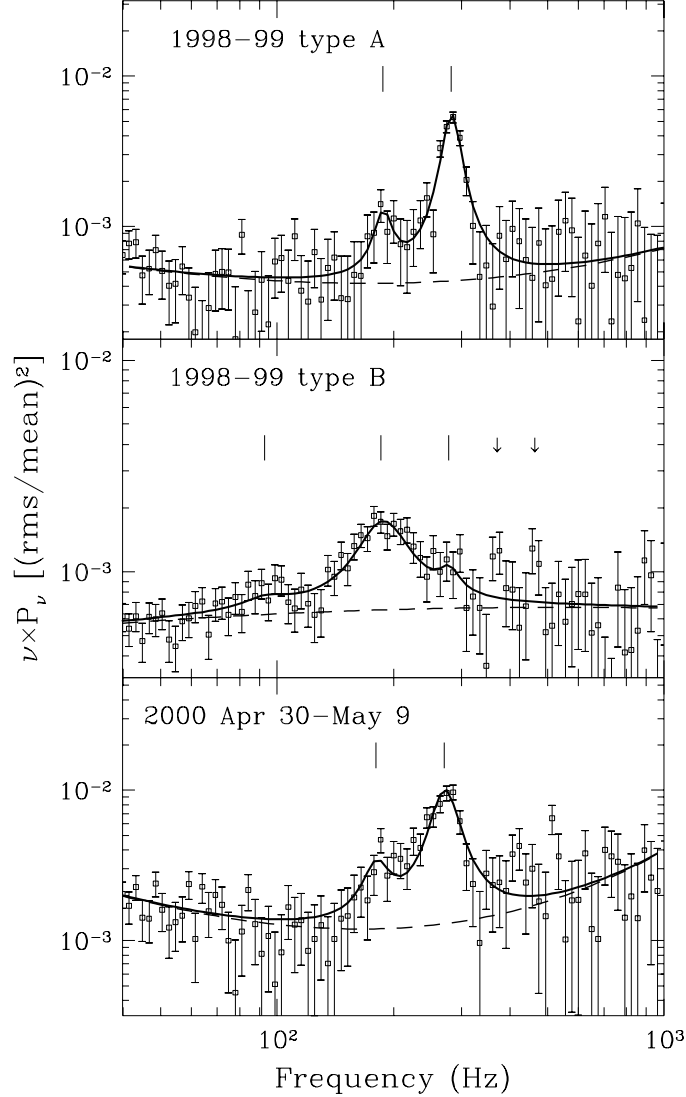


Fig. 2.— Fits for harmonically related HFQPOs in XTE J1550–564 applied to power spectra at 6–30 keV. The top two panels show the same data displayed in Fig. 1 (1998–1999 averages for LFQPO types A and B). The bottom panel shows the QPO fit for the average of 12 observations made between 2000 April 30 and May 9. In each panel, the tick marks above the data show the central frequencies of the significant QPOs. The best fit is shown with a smooth, dark curve, and the power continuum is shown with a dashed line. For the type B group (middle panel), the arrows show the expected locations of the 4th and 5th harmonics.



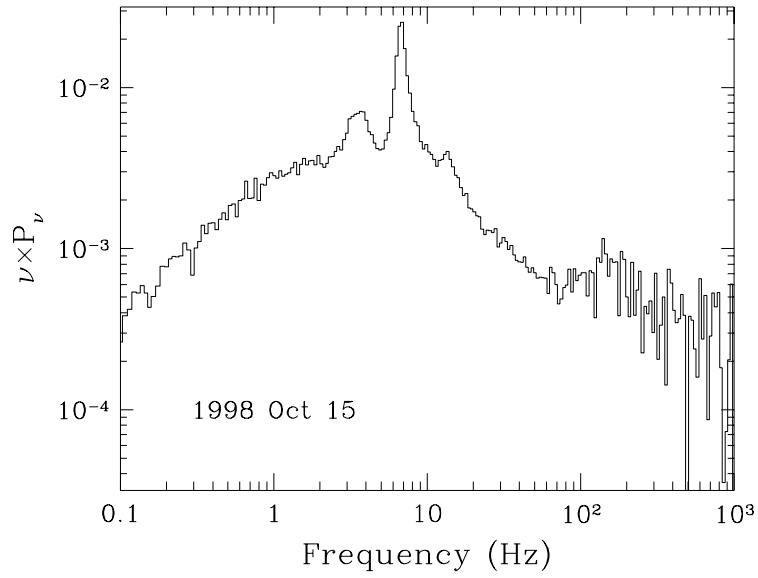


Fig. 3.— Histogram of HFQPO frequencies for XTE J1550–564 and GRO J1655–40. The binning intervals are varied to maintain a width of  $\pm 5\%$  relative to the central frequency. Each source displays two peaks in the distribution that have a 3:2 ratio in frequency.

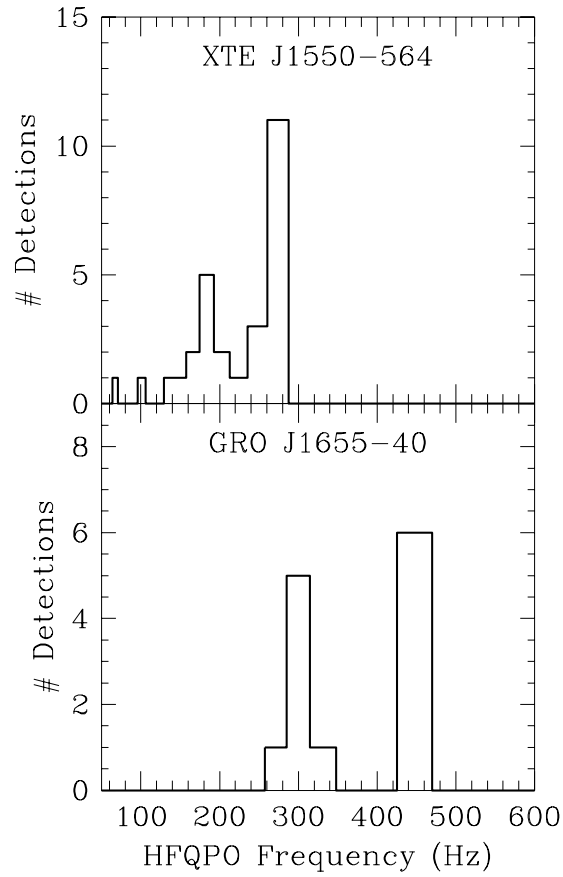


Fig. 4.— Average power spectrum for XTE J1550–564 for the two observations made on 1998 October 15. The QPO at  $143 \pm 8$  Hz represents the most significant deviation from the harmonic scheme (92, 184, 276 Hz) that accounts for most of the HFQPO detections in this source.

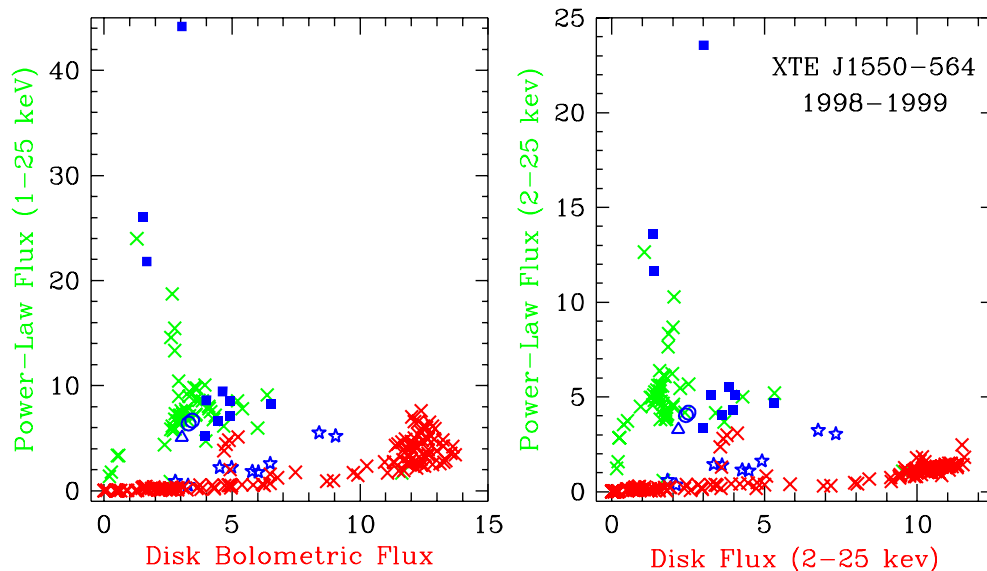


Fig. 5.— Energy spectrum deconvolution for XTE J1550–564 during the 1998–1999 outburst. The flux from the accretion disk and the X-ray power law are shown in conventions of both bolometric flux (extrapolated; left) and apparent flux (2–25 keV; right). The color of the plotting symbol denotes the QPO conditions: HFQPO detections (blue), only LFQPOs (green “x”), and no QPOs (red “x”). In addition, the shape of the blue symbols distinguishes the HFQPOs near 92 Hz (triangle), 184 Hz (filled square), and 276 Hz (star). The pair of observations on 1998 October 15 are displayed with blue circles. In either flux convention, there is a systematic shift away from disk-dominated track (red x’s) as the detected HFQPO shifts from 276 to 184 Hz.

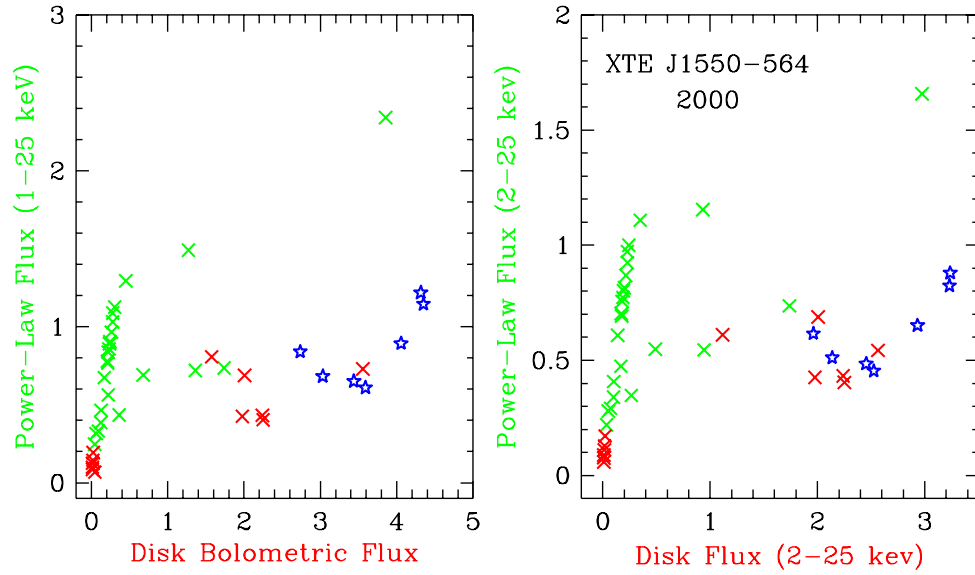


Fig. 6.— Energy spectrum deconvolution for XTE J1550–564 during the outburst of 2000. The symbols follow the definitions given for Fig. 4. In this outburst there is a track in which the power-law spectrum dominates (green x’s), and the points associated with HFQPOs near 276 Hz (blue stars) are again close to the disk-dominated track shown in Fig. 4.

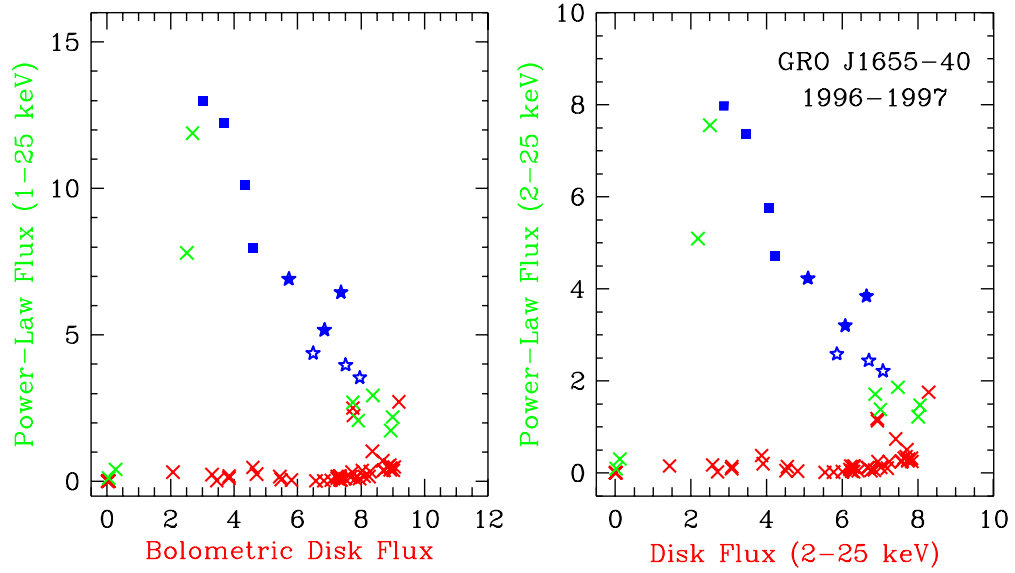


Fig. 7.— Energy spectrum deconvolution for GRO J1655–40 during its outburst of 1996–1997. The symbols follow the definitions given for Fig. 4, except that the observations that exhibit both HFQPOs (300 and 450 Hz) are shown with solid stars. The results are very similar to those for XTE J1550–564 (Fig. 4). There is increasing power-law flux as the strongest HFQPO shifts from the 450 Hz feature (open stars) to the 300 Hz feature (solid squares).

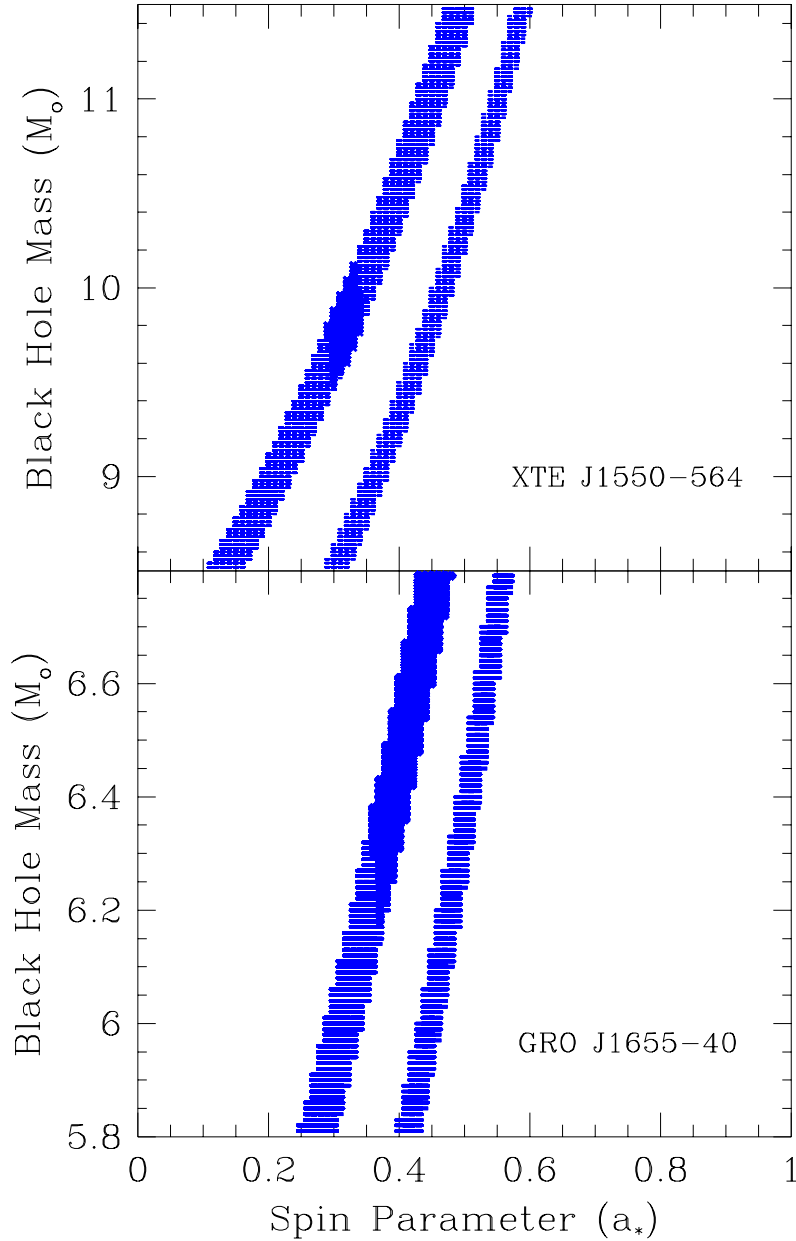


Fig. 8.— Application of the coordinate-frequency resonance model to the HFQPOs in XTE J1550–564 (top) and GRO J1655–40 (bottom). At each point in the blue shaded regions, the orbital and radial frequencies are within 2% of the HFQPO harmonic frequencies. In each panel, the left track corresponds with the 2:1 resonance (i.e. 184 : 92 Hz in the top panel and 300 : 150 Hz in the bottom panel), and the right track corresponds with the 3:1 resonance (276 : 92 Hz and 450 : 150 Hz, respectively). The regions shaded with darker blue show the parameters that additionally yield a frame-dragging frequency in the range of 5.8-6.4 Hz (top) and 12.2-17.5 Hz (bottom). We caution that the association of LFQPOs with the frame-dragging frequency is highly speculative.

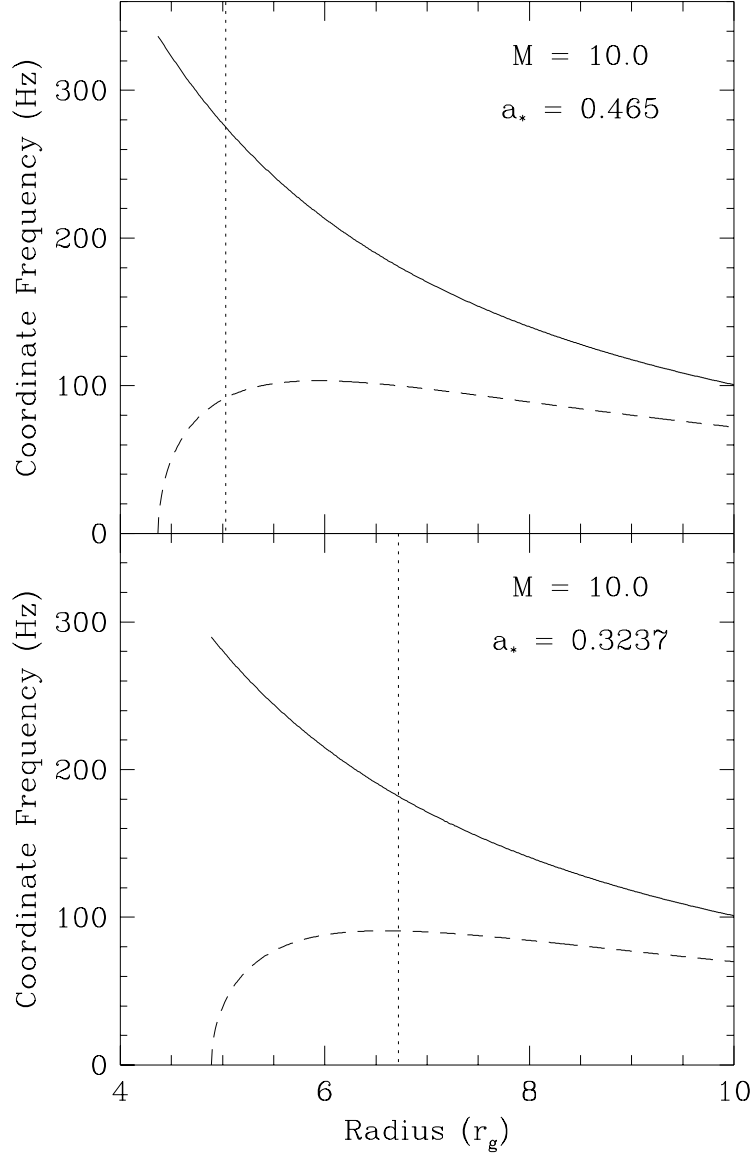


Fig. 9.— Frequencies predicted by GR as a function of radius, for cases that illustrate a 3:1 resonance (top) and a 2:1 resonance (bottom) between the orbital (solid curve) and radial (dashed curve) coordinate frequencies. In each case the mass is  $10 M_\odot$  and the spin parameter has been chosen to match the resonances to the values 276:92 Hz and 184:92 Hz, respectively. In each case, the gradients in the coordinate frequencies have opposite signs, and this creates a narrow region in radius where the frequency ratio is near an integral value. Shifts in the observed frequencies may therefore be very difficult to accommodate in the resonance model, especially for the 3:1 resonance.